ELSEVIER

Journal of Nuclear Materials 278 (2000) 54–63

journal of nuclear materials

www.elsevier.nl/locate/jnucmat

Rim structure formation and high burnup fuel behavior of large-grained UO_2 fuels

K. Une [a,*], M. Hirai [a], K. Nogita [a], T. Hosokawa [a], Y. Suzawa [b], S. Shimizu [c], Y. Etoh [d]

[a] *Nippon Nuclear Fuel Development Co. Ltd., 2163 Narita-cho, Oarai-machi, Higashi Ibaraki-gun, Ibaraki-ken 311-1313, Japan*
[b] *Tokyo Electric Power Co., Egasaki-cho 4-1, Tsurumi-ku, Yokohama, Kanagawa-ken 230-8510, Japan*
[c] *Toshiba Co., Shinsugita-cho 8, Isogo-ku, Yokohama, Kanagawa-ken 235-8523, Japan*
[d] *Hitachi Ltd., Saiwai-cho 3-1-1, Hitachi-shi, Ibaraki-ken 317-8511, Japan*

Received 24 May 1999; accepted 11 August 1999

Abstract

Irradiation-induced fuel microstructural evolution of the sub-divided grain structure, or rim structure, of large-grained UO_2 pellets has been examined through detailed PIEs. Besides standard grain size pellets with a grain size range of 9–12 μm, two types of undoped and alumino-silicate doped large-grained pellets with a range of 37–63 μm were irradiated in the Halden heavy water reactor up to a cross-sectional pellet average burnup of 86 GWd/t. The effect of grain size on the rim structure formation was quantitatively evaluated in terms of the average Xe depression in the pellet outside region measured by EPMA, based on its lower sensitivity for Xe enclosed in the coarsened rim bubbles. The Xe depression in the high burnup pellets above 60 GWd/t was proportional to $d^{-0.5}$–$d^{-1.0}$ (d: grain size), and the two types of large-grained pellets showed remarkable resistance to the rim structure formation. A high density of dislocations preferentially decorated the as-fabricated grain boundaries and the sub-divided grain structure was localized there. These observations were consistent with our proposed formation mechanism of rim structure, in which tangled dislocation networks are organized into the nuclei for recrystallized or sub-divided grains. In addition to higher resistance to the microstructure change, the large-grained pellets showed a smaller swelling rate at higher burnups and a lower fission gas release during base irradiation.

PACS: 28.41.B; 61.80

1. Introduction

In order to reduce the amount of spent fuels and to improve the fuel cycle cost, maximum fuel discharge burnup of light water reactors (LWRs) in Japan has been extended step-by-step [1]. When extending fuel burnup, fission gas release and fission gas bubble swelling are of practical importance in determining the performance of high burnup fuel rod, due to the impact on fuel rod internal pressure and pellet-cladding interaction (PCI). Moreover, fuel microstructural change of the sub-divided grain structure, or rim structure, becomes remarkable for the peripheral region of UO_2 pellets at higher burnups above 35–40 GWd/t, with the structure developing into the pellet inside region on increasing the burnup [2–8]. This rim structure is characterized by a marked decrease in the UO_2 grain size and an increase in porosity due to newly formed coarsened bubbles. From detailed microstructure examinations, mainly by transmission electron microscopy (TEM), the rim structure has been clarified to be fission-induced recrystallization due to the accumulation of radiation damage, and we have proposed the framework of the formation mechanism [9–11]. This microstructure change must influence fuel performance at high burnup through the increases of fission gas release, fuel swelling and fuel temperature [7].

* Corresponding author. Tel.: +81-29 267 9012; fax: +81-29 266 2589.
E-mail address: une@nfd.co.jp (K. Une).

0022-3115/00/$ - see front matter
PII: S0022-3115(99)00214-7

The application of large-grained UO_2 pellet has been considered as a means to suppress fission gas release and intergranular bubble swelling at high burnups [12–15], because of the longer diffusion distance of fission gas atoms and the smaller grain boundary area which provides precipitation sites for bubbles. It is also anticipated from the proposed formation mechanism of rim structure [9,11] that large grain structure can also affect the microstructure change. In fact, recently some good results have been reported. One result was SEM fractographs which showed localized rim formation near the grain boundaries in a PWR pellet irradiated to 67 GWd/t [16] and another was our TEM observations which showed less rim structure formation in large-grained pellets irradiated to 60 GWd/t [17]. However, no systematic assessment has been made on the effect of grain size on microstructure change and integrated fuel behavior at higher burnups above 60 GWd/t.

In this study, two types of large-grained UO_2 fuels with and without alumino-silicate addition, and standard fuel, all of which had been irradiated to rod average burnups of 25–75 GWd/t (pellet peak burnup: 33–86 GWd/t) in the Halden heavy water reactor (HBWR), were subjected to detailed microstructural examinations and analyses. The effect of large grain structure on the rim structure formation and high burnup fuel behavior of fuel swelling and fission gas release were clarified.

2. Experimental

2.1. Fuel design and irradiation

Two types of fuel rods of different designs were installed into two irradiation rigs, IFA551 and IFA566, and were provided for the irradiation tests in the HBWR. The two rigs consisted of BWR 9×9 type fuel rods (IFA551) and small diameter fuel rods (IFA566). The latter rods have been aimed at accelerating fuel burnup in a shorter irradiation period, using higher enriched pellets. Each rod was equipped with in-reactor instrumentation (a pressure transducer and/or a fuel stack elongation gauge). The fuel rod specifications are summarized in Table 1. The uranium was enriched to 8 and 13 wt% ^{235}U for 9×9 type fuel rods and small diameter fuel rods, respectively.

Besides the standard grain size pellet, several types of improved pellets were fabricated and loaded in these fuel rods. Among them, the data of two types of undoped and alumino-silicate doped large-grained pellets are reported in this paper. The three-dimensional grain size (conversion factor from two-dimensional value obtained by ceramography: 1.56) and sintered density of the three types of pellets are given in Table 2. The density for all the pellets was high at 97–98% TD, and the grain size was 9–12 μm for the standard pellet, 51–63 μm for the undoped large-grained pellet and a wide range of 37–58 μm for the synthetic alumino-silicate doped pellet, depending on the additive concentration of 0.025–0.25 wt%. The composition of the alumino-silicate was 60 wt% SiO_2–40 wt% Al_2O_3. The ceramographs of as-fabricated pellets of standard, undoped large-grained and 0.25 wt% alumino-silicate doped are shown in Fig. 1. Alumino-silicate segregates in the grain boundaries and forms a liquid phase during the sintering process, which enhances sintering and grain growth. In the two large-grained pellets, larger pores precipitate both in grains and on grain boundaries, compared to the morphology of the standard pellet. Other information on the rod design and pellet fabrication was described in detail previously [13,15].

Table 1
Fuel rod specifications

		BWR 9×9 type fuel (IFA551)	Small diameter fuel (IFA566)
Pellet	Outside diameter (mm)	9.6	5.5
	Height (mm)	9.6	5.5
	Enrichment (%)	8	13
Cladding	Cladding type	Zr liner	Zr liner
	Outer diameter (mm)	11.2	6.5
Rod	Stack length (mm)	400	240
	Diametral gap (mm)	0.20	0.11
	He pressure (MPa)	1	1

Table 2
Grain size and density of UO_2 fuel pellets

Pellet type	Grain size (μm)	Density (% TD)
Undoped standard grain	9–12	96.8–97.2
Undoped large-grained	51–63	96.4–96.9
Al–Si–O doped large-grained	37–58	97.1–97.8

The IFA551 rig had two clusters of upper and lower, while the IFA566 rig three clusters of upper, middle and lower. The average linear heat rating of rods was around 300–470 W/cm up to average burnups of 25 and 53 GWd/t for the former rig, and around 200–400 W/cm up to average burnups of 30–75 GWd/t for the latter rig. The corresponding pellet peak burnups were 25 and 62 GWd/t for the former, and 38–86 GWd/t for the latter. Simplified irradiation data are given in Table 3. Details of the power histories of each rod were described elsewhere [13,15].

2.2. Post irradiation examinations (PIEs)

The fuel specimens subjected to detailed PIEs were mainly taken from the peak burnup locations of each rod. The fuel microstructure was examined by optical microscopy (OM) and scanning electron microscopy (SEM) on a polished surface, by SEM on a fractured surface prepared by diamond scratch method and by TEM on an argon ion thinned specimen. Details of the TEM experiments have been described elsewhere [10,11]. Fission products (FPs) of Xe and Ce retained in the fuel were analyzed by electron probe microanalysis (EPMA) with an electron beam diameter of 30 μm. Relative FP concentrations were obtained by dividing each characteristic X-ray intensity by that of uranium at the same location, so as to eliminate any effect from irregularity of the specimen surface. Fission gas release during base irradiation was evaluated by pin puncture test and retained gas measurement in the pellets by a dissolution method into nitric acid. Fuel swelling was examined by immersion density measurement using meta-xylene.

3. Results and discussion

3.1. Rim structure formation

3.1.1. Evaluation of rim structure

From our previous examinations [7,9–11] of X-ray diffractometry, SEM and TEM on high burnup fuels, we

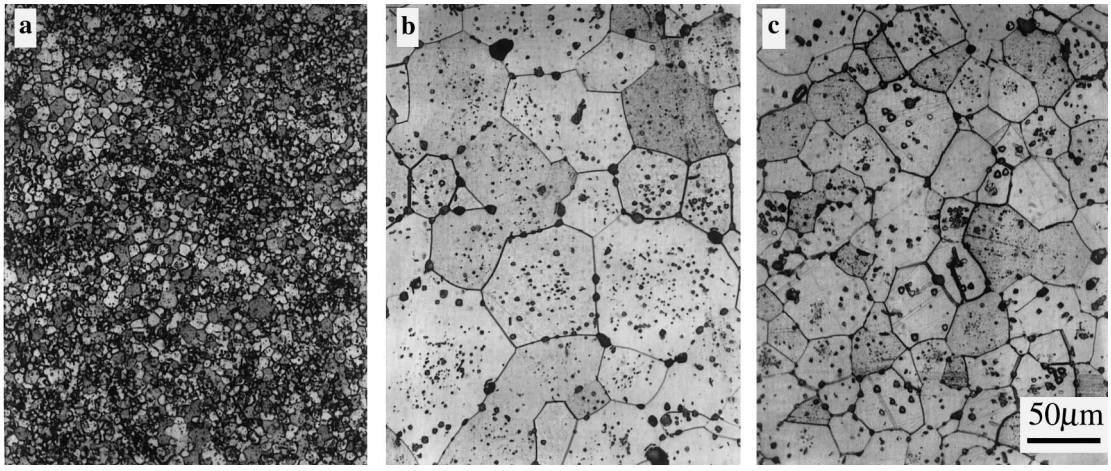

Fig. 1. Ceramographs of as-fabricated UO_2 fuels: (a) standard grain fuel (grain size: 9 μm), (b) undoped large-grained fuel (grain size: 51 μm), (c) Al–Si–O doped large-grained fuel (grain size: 46 μm).

Table 3
Irradiation conditions of IFA551 and IFA-566 rigs[a]

Irradiation cluster	Rod average burnup (GWd/t)	Pellet peak burnup (GWd/t)	Average LHGR (W/cm)		
			BOL	MOL	EOL
IFA551 (upper)	25	33	470	400	350
IFA551 (lower)	53	63	470	380	300
IFA566 (lower)	30	38	250	230	220
IFA566 (middle)	60	61	350	350	300
IFA566 (middle)	63	64	420	360	360
IFA566 (upper)	75	86	240	200	170

[a] BOL: beginning of life; MOL: middle of life; EOL: end of life.

have proposed the formation mechanism of the rim structure originating from the accumulation of radiation damage. Tangled dislocation networks are formed by the inhomogeneous accumulation of dislocations after the development of interstitial-type dislocation loops. On the other hand, intragranular fission gas bubbles are formed by the clustering of vacancies and fission gas atoms. When increasing burnup, the tangled dislocations are organized into sub-grains of 20–30 nm in size with high angle boundaries and they are regarded as the nuclei for recrystallization. Then, the coarsened bubbles are formed by sweeping out of fission gas atoms and small intragranular bubbles during grain growth on recrystallization, and by short circuit diffusion of fission gas atoms along recrystallized grain boundaries. Therefore, the coarsened rim bubbles have been considered to retain fission gases of Xe and Kr at high pressure [2,7,18]. The driving force for nucleus grain growth would be supplied mainly by strain energy induced by radiation damage.

The rim structure formation has been recognized in terms of the porous region by OM and/or SEM, the sub-divided grain structure by SEM fractography, the recrystallized grains by TEM and the fractional Xe depression by EPMA. The last technique originates from the significant lowering of EPMA sensitivity for Xe enclosed in the rim bubbles [19]. Among the above techniques, radial distributions of porosity and Xe concentration are suitable for the quantitative evaluation of rim structure formation in the pellet outside region, since both phenomena are directly related to the formation of coarsened rim bubbles. Although the fractional recrystallized area obtained from TEM is straightforward, the observation area is very small and limited. Therefore, in the present study, the average Xe depression in the pellet outside region was adopted as an index of the extent of rim structure formation.

3.1.2. IFA551 fuels

In the IFA551 rig, BWR 9×9 type fuel rods were irradiated up to rod average burnups of 25 and 53 GWd. From each rod, fuel specimens with cross-sectional average burnups of 33 and 61 GWd/t were prepared. No Xe depression or sub-divided grain structure was confirmed for any outside region of the 33 GWd/t pellets by EPMA and SEM examinations. The radial Xe profiles for the three types of 61 GWd/t pellets are shown in Fig. 2. The relative concentration of Xe was normalized by that of U from the same location to eliminate the effect of irregularity in the surface condition (due to large pore and cracks). This figure also shows the generated Xe profile which was estimated by using the simultaneously measured Ce profile, which represents the relative burnup profile, and the relationship between characteristic X-ray intensity of Xe measured in the pellet outside region and specimen burnup.

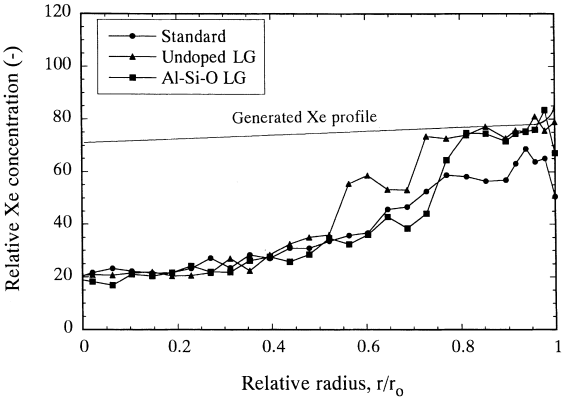

Fig. 2. Comparison of radial Xe distributions between standard and large-grained fuel pellets irradiated to 61 GWd/t in IFA551 rig. Standard: standard fuel; undoped LG: undoped large-grained fuel; Al–Si–O LG: Al–Si–O doped large-grained fuel.

The latter correlation had been established in advance for UO_2 fuels of the present and other projects irradiated to the burnups below 60 GWd/t in the HBWR. The generated Xe profile is almost flat, except for about 10–15% enhanced concentration close to the pellet edge. This enhancement is much smaller than that (about 150–200%) of pellets irradiated in LWRs [2–8]. Namely, Pu buildup by epithermal neutron captures of ^{238}U at the pellet peripheral region is considerably suppressed in the present pellets compared to the case of LWR pellets, because of the use of the highly enriched U in the present experiments and softer neutron spectrum in the HBWR.

Significant depression of Xe in the high temperature region of $r/r_o = 0$–0.7 corresponds to thermally activated fission gas release from the pellet during base irradiation of 300−450 W/cm. On the other hand, the depression observed in the outer region of $r/r_o = 0.8$–1.0 for the standard pellet is attributable to the precipitation of coarsened rim bubbles. Comparing the average Xe depressions in that region among these specimens, the value (21%) for the standard pellet is much larger than that (2–3%) for the two types of large-grained pellets. These EPMA results clearly demonstrate that the large-grained pellets have high resistance to microstructure change. Ceramographs and SEMs on the polished and etched surface of the 61 GWd/t fuels also showed the formation of coarsened rim bubbles only for the standard pellet.

3.1.3. IFA566 fuels

In the IFA566 rig, small diameter fuel rods were irradiated up to rod average burnups of 30, 60, 63 and 75 GWd. From each rod, fuel specimens with average burnups of 30, 60, 63 and 86 GWd/t were prepared. No

Xe depression or sub-divided grain structure in the pellet outer region was confirmed for any of the 30 GWd/t pellets, while some Xe depression was observed for the other high burnup pellets.

The radial Xe profiles for the three types of 60 GWd/t pellets are shown in Fig. 3. As seen in the case of the 61 GWd/t pellets of IFA551, the depression observed in the outer region ($r/r_o = 0.8$–1.0) for the standard pellet is attributed to the formation of rim structure. Comparing the average Xe depression in that region among three specimens, the value (23%) for the standard pellet is about three times larger than that (8%) for the two types of large-grained pellets. This result is qualitatively consistent with TEM results for these pellets, which has been reported in the previous paper [17]. The TEM specimens were prepared from the pellet periphery. Namely, fraction of recrystallization (the ratio of recrystallized structure in the total TEM observation area, excluding coarsened bubbles) is in the same order: 30% for the standard and 8% for the two large-grained pellets [17]. As a reference, this value at the pellet peripheral location of a commercial BWR fuel (local burnup: 100 GWd/t) is 40% [11]. Fig. 4 shows the correlation between the fraction of recrystallization and Xe depression for the IFA566 pellets of 60 GWd/t and the BWR pellet. A relatively good linear relationship proves that the Xe depression detected by EPMA is directly linked with the recrystallized process. A similar Xe behavior was observed for the 63 GWd/t pellets. Namely, the average Xe depression of 16% for the Al–Si–O doped large-grained pellet is smaller than the value of 26% for the standard pellet. These EPMA and TEM results clearly demonstrate that the large-grained pellets have high resistance to microstructure change.

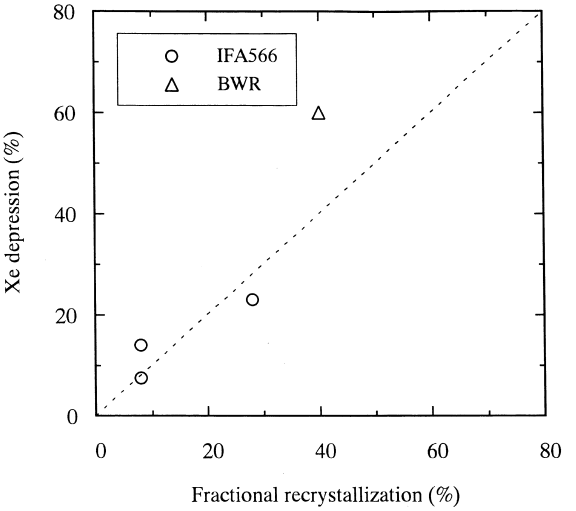

Fig. 4. Relationship between fractional recrystallization observed by TEM and Xe depression measured by EPMA.

By comparing the data of the two types of fuels with the different fuel rod specifications in IFA551 and IFA566 rigs, the effects of pellet size and fission rate could be identified. The fission rate for the small diameter rods in IFA566 rig was about three times higher than that for the BWR 9×9 type rods in IFA551 rig, since the linear heat rates of fuel rods in both rigs were roughly equivalent to each other. Almost the same Xe depressions in the pellet outside region for the two types of standard pellets shown in Figs. 2 and 3 prove that pellet size and fission rate have hardly any effect.

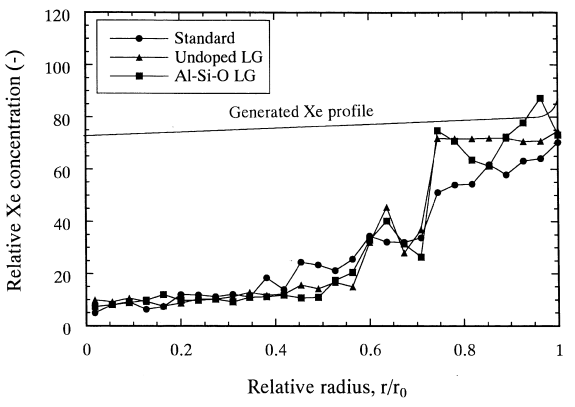

Fig. 3. Comparison of radial Xe distributions between standard and large-grained fuel pellets irradiated to 60 GWd/t in IFA566 rig. Standard: standard fuel; undoped LG: undoped large-grained fuel; Al–Si–O LG: Al–Si–O doped large-grained fuel.

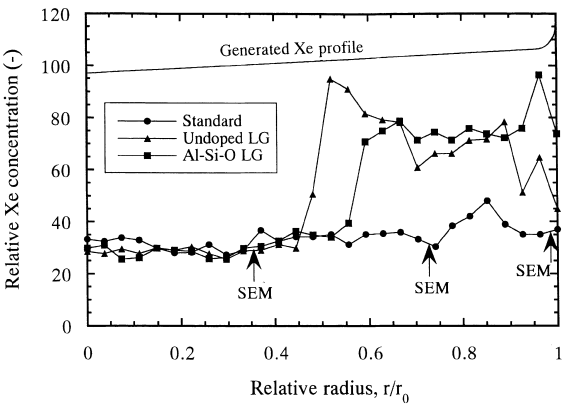

Fig. 5. Comparison of radial Xe distributions between standard and large-grained fuel pellets irradiated to 86 GWd/t in IFA566 rig. Standard: standard fuel; undoped LG: undoped large-grained fuel; Al–Si–O LG: Al–Si–O doped large-grained fuel.

The corresponding Xe profiles for the 86 GWd/t pellets are shown in Fig. 5. These pellets were base-irradiated at lower powers of 170–240 W/cm than those for the 60 GWd/t pellets shown in Fig. 3. The Xe depressions in the pellet middle to center region ($r/r_o = 0$–0.5) are not larger than those of the 60 GWd/t pellets, because of their lower linear heat rates. By contrast, in the pellet middle to rim region ($r/r_o = 0.5$–1.0), remarkable differences are seen between the standard and large-grained pellets. In particular, an almost flat Xe profile is detected in a whole region for the standard pellet, while the Xe concentration for the two large-grained pellets increases around the location of $r/r_o = 0.5$–0.6. The significant Xe depression in the outside region of the former pellet is obviously due to a highly developed rim structure formation. Actually, SEM fractographs for this pellet (Fig. 6) show the developed sub-divided grain structure, even in the pellet inside region of $r/r_o = 0.35$. Naturally, the degree of sub-grain structure appears to become less toward the inner region of the pellet. In Fig. 7, the SEM fractographs for the alumino-silicate doped large-grained pellet are shown, in which the developed sub-grain formation is limited in the peripheral region, and less microstructure change is seen in other regions. Eventually, the values of average Xe depression in the pellet outside region of $r/r_o = 0.7$–1.0 are 63% for the standard pellet, 35% for the undoped large-grained pellet and 25% for the alumino-silicate doped large-grained pellet, indicating that the last pellet has the best rim structure resistance.

3.1.4. Effect of grain size

Burnup dependence of the average Xe depression in the pellet outside region obtained in the present IFA series is summarized in Fig. 8. In the figure, least squares curves fitted by Weibull functions are also presented. In the functions, the maximum depression was assumed to be 85%, based on the measured values in the fuel specimens irradiated to local burnup more than 100 GWd/t [20,21]. With increasing grain size, rim structure development rate is suppressed, and the Xe depressions at 86 GWd/t for the large-grained pellets are about half of the value for the standard grain size pellet.

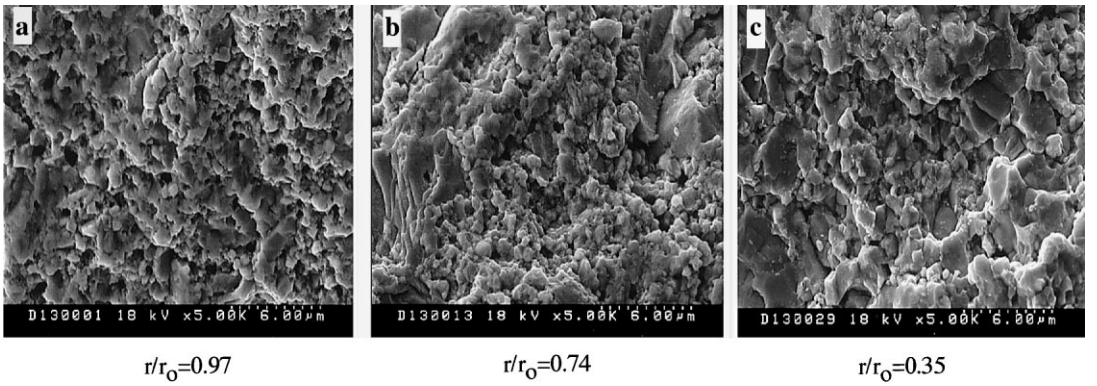

Fig. 6. SEM fractographs of standard grain size fuel irradiated to 86 GWd/t: (a) $r/r_o = 0.97$, (b) $r/r_o = 0.74$, (c) $r/r_o = 0.35$.

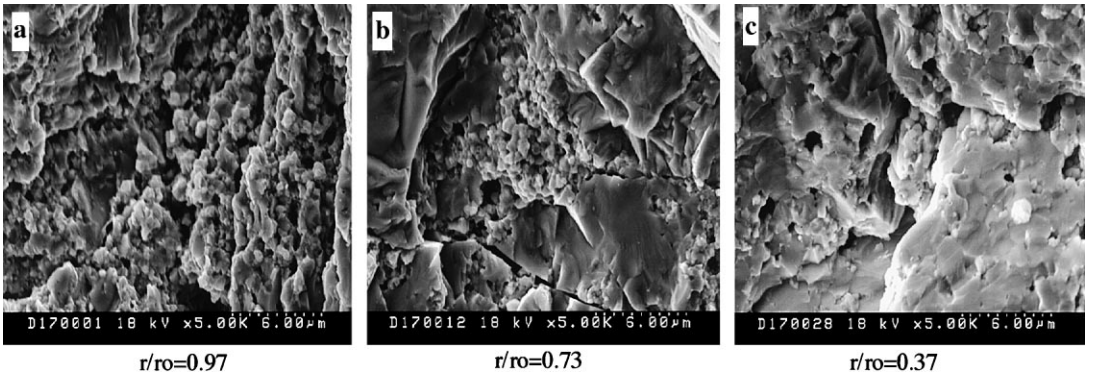

Fig. 7. SEM fractographs of Al–Si–O doped large-grained fuel irradiated to 86 GWd/t: (a)$r/r_o = 0.97$, (b) $r/r_o = 0.73$, (c) $r/r_o = 0.37$.

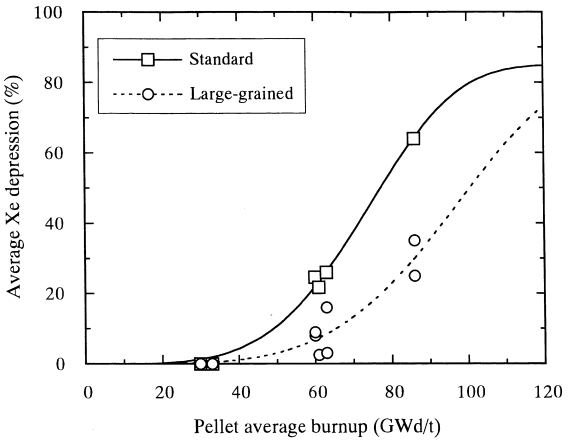

Fig. 8. Burnup dependence of average Xe depression in pellet outside region for fuel pellets irradiated in IFA551 and IFA566 rigs.

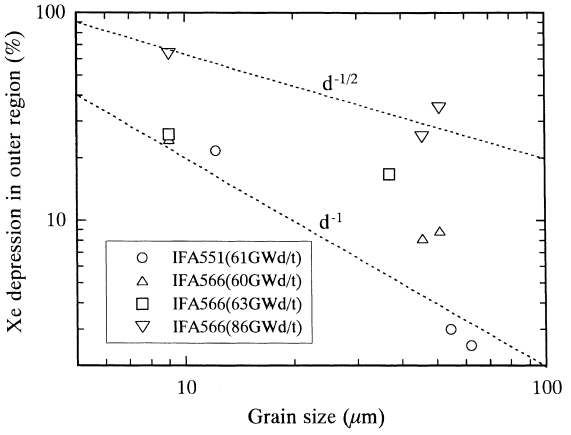

Fig. 9. Grain size dependence of average Xe depression in pellet outside region.

Fig. 9 plots the grain size dependence of the Xe depression measured by EPMA for the IFA551 fuels of 61 GWd/t and IFA566 fuels with three different burnups of 60, 63 and 86 GWd/t. For the 60 GWd/t pellet of IFA566 and 61 GWd/t pellet of IFA551, the average Xe depressions are roughly proportional to $d^{-0.75}$–$d^{-1.0}$ (d: grain size). For the 63 and 86 GWd/t pellets of IFA566, the relationship, the average Xe depression $\propto d^{-0.5}$, is derived. Generally with increasing burnups, the grain size dependency seems to weaken from $d^{-1.0}$ to $d^{-0.5}$.

A mechanistic explanation for this grain size effect is supported by the following microstructure examinations. TEM images of Fig. 10, obtained from the standard and Al–Si–O doped large-grained pellets of 33 GWd/t (IFA551), clearly demonstrate an inhomogeneous accumulation of dislocations along the grain boundaries. This indicates that the grain boundaries inhibit climbing motion of dislocations and then are important sites for inhomogeneous dislocation accumulation, namely for formation of nuclei for recrystallization. Our previous TEM image for a 83 GWd/t fuel also showed a high density of dislocations decorated the as-fabricated grain boundaries [9]. Consequently, a smaller as-fabricated grain size leads to a higher dislocation density since there is a larger grain boundary surface area per volume. From a simple geometrical consideration, the grain boundary area per volume is inversely proportional to grain size, i.e. $\propto d^{-1.0}$. Fig. 11 shows the ceramographs of as-etched surface for the standard and Al–Si–O doped large-grained pellets of 86 GWd/t (IFA566), in which the coarsened rim bubbles are localized near the boundaries, especially for the large-grained pellet. Also in Fig. 7 of SEM fractograph at $r/r_o = 0.74$ for the large-grained pellet, sub-divided grain structure appears to be localized along the boundaries.

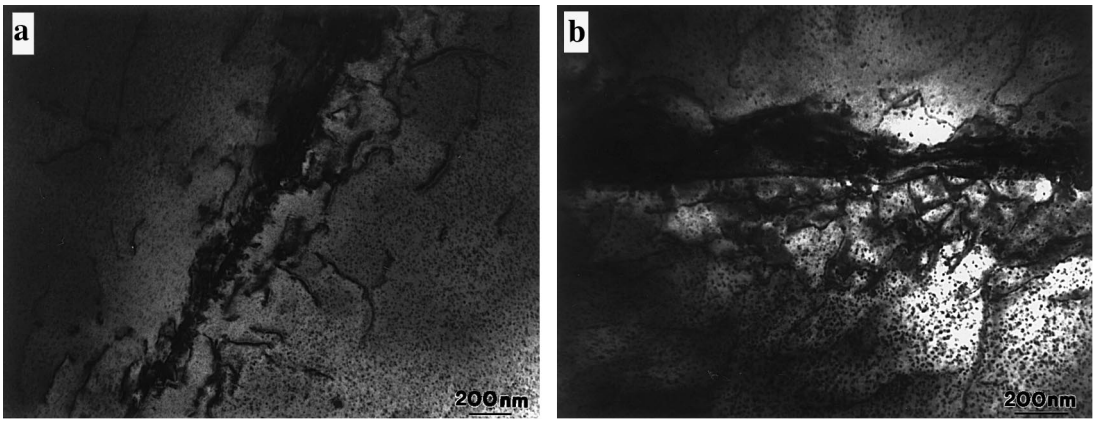

Fig. 10. Bright-field TEM images in pellet outside region of fuels irradiated to 33 GWd/t in IFA551 rig: (a) standard fuel, (b) Al–Si–O doped large-grained fuel.

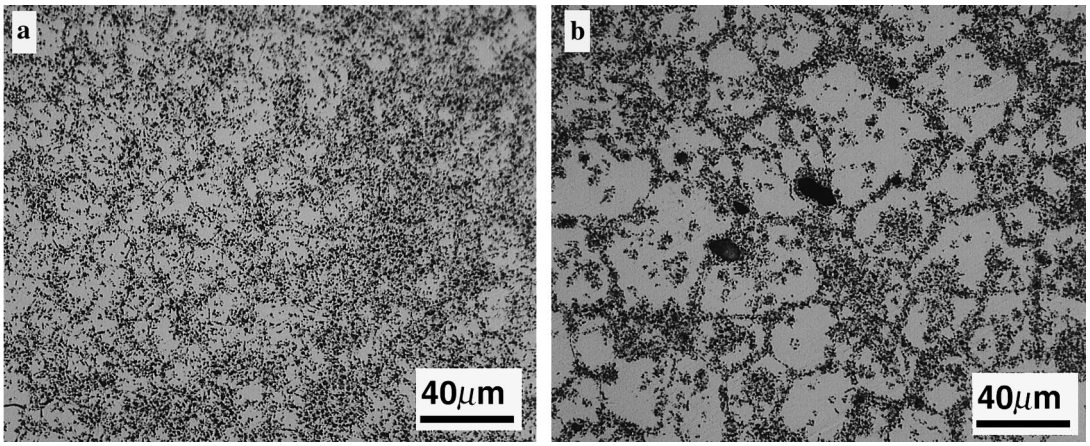

Fig.11. Ceramographs at $r/r_o = 0.74$ on as-etched surface of fuels irradiated to 86 GWd/t in IFA566 rig: (a) standard fuel, (b) Al–Si–O doped large-grained fuel.

3.2. High burnup fuel behavior

3.2.1. Fuel swelling

Fuel swelling is directly related to PCI performance of a fuel rod. In Fig. 12, density change of the fuel pellets is plotted against pellet average burnup which was evaluated by immersion density measurements. The solid line indicates a matrix swelling rate of 0.5%/10 GWd/t, which has been sometimes applied to commercial reactor fuels irradiated up to 40–50 GWd/t [22–25]. In these fuels with initial densities of 94–96% TD, densification of about 0.5–1% occurs at low burnups below 10 GWd/t, followed by the above swelling rate. Then, at high burnups above 50 GWd/t, swelling rate appears to increase beyond the solid line, and approaches the dotted line of matrix swelling plus rim bubble swelling. The rim swelling was estimated from the burnup dependence of rim width and an average rim porosity of 7% in the restructured region [7], which is based on the reported maximum total porosity (as-fabricated porosity plus rim porosity) of 15–25% at the pellet edge [3,16].

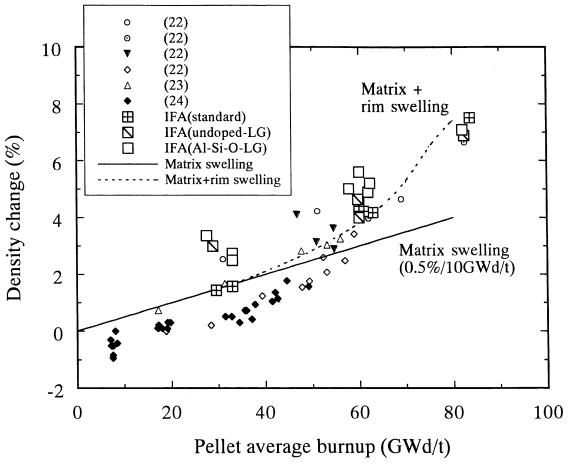

Fig. 12. Burnup dependence of fuel swelling.

In the case of the present three types of IFA pellets with high densities of 97–98% TD, the fuel swelling of the large-grained pellets at the middle burnup of about 30 GWd/t is 1–1.5% larger than that of the standard pellet, which can be fitted just on the solid line of the matrix swelling rate of 0.5%/10 GWd/t. This indicates that the initial swelling rate of the large-grained pellets is about 1%/10 GWd/t, double the value of the standard pellet. This increased initial swelling rate for the large-grained pellets is attributable to the almost zero densification and fewer accommodation sites of small pores for fission gases and solid FPs. When increasing burnup up to 60–80 GWd/t, the swelling rate for the standard pellet appears to follow the dotted matrix plus rim swelling curve, and eventually no significant difference is found for the three types of pellets at high burnups. Moreover, it must be noted that the swelling of the standard pellets at high burnups would be somewhat underestimated. This reason originates from the fact that the complete removal of the pellets from the fuel rod was difficult for density measurements in comparison with the large-grained pellets, because of a severe pellet-cladding bonding seen in the former pellet. The lower swelling rate of the large-grained pellets at high burnup is related to their milder microstructure change.

3.2.2. Fission gas release

Fission gas release during base irradiation was evaluated by pin puncture test and dissolution test for the two different rods irradiated to 25 and 53 GWd/t in IFA551 rig and for the three different rods irradiated to

30, 60 and 75 GWd/t in IFA566 rig. The data from the latter technique were more reliable for the high burnup fuel rods of 60 and 75 GWd/t since formation of the pellet-cladding bonding layer blocked gas transport from the active stack region to the gas collecting head of the puncture machine.

The finally evaluated fission gas releases for the IFA551 fuel rods of 25 GWd/t are 11.1%, 6.9% and 7.3% for the standard, undoped large-grained and alumino-silicate doped large-grained fuels, respectively, and the corresponding values from the 53 GWd/t rods are 13.6%, 4.5% and 7.6% for them. In the case of the IFA566 fuels, they are 2.0%, 1.3% and 1.2% for the 30 GWd/t rods, 42.2%, 31.1% and 28.1% for the 60 GWd/t rods, and 13.6%, 6.8% and 8.5% for the 75 GWd/t rods. All the large-grained rods irradiated in IFA551 and IFA566 rigs show lower fission gas releases than those for the standard rods with the same irradiation histories. Relative values of fission gas release from the present IFA551 and IFA566 experiments are summarized in Fig. 13 as a function of reciprocal grain size when the values for the standard rods are set at unity. The gas releases from the large-grained fuels are about 50–70% of the standard rod values, roughly irrespective of fuel burnup.

According to the simple diffusion model of fission gas atoms [26], the fractional fission gas release is inversely proportional to grain size when the release value is below about 30%. Thus this model predicts that fission gas releases from the large-grained fuels (grain size: 36–56 μm) are about 20–25% of those from the standard fuel (9–12 μm). However, the PIE data are not in agreement; they show fraction of 50–70%. This inconsistency may result from: (1) the applicability of the simple diffusion model (when the fractional release is beyond 30%, the grain size dependence becomes weaker), and (2) the grain growth effect during base irradiation. In fact, the grain size of the standard pellet of 60 GWd/t increased to about three times the initial one in the central region of pellet. On the other hand, grain growth did not appear in the large-grained pellets. In addition to the above thermally activated (or diffusion-controlled) release process from high temperature region, a part of the fission gasses certainly release from low temperature rim structure region via non-thermally activated process. Actually, about 10–20% of generated amount of fission gases have been reported to be lost from the rim structure region and to release into the rod free volume [8].

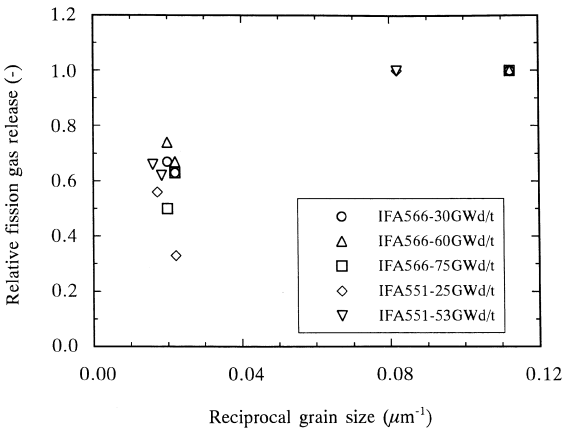

Fig. 13. Grain size dependence of relative fission gas release during base irradiation.

4. Conclusions

Rim structure formation and high burnup fuel behavior of large-grained UO_2 pellets were systematically examined through detailed PIEs. Three types of fuel pellets (standard grain size, undoped large-grained, alumino-silicate doped large-grained) were loaded into two different types of rigs, and irradiated in the HBWR to rod average burnups of 25–75 GWd/t (pellet peak burnups: 33–86 GWd/t).

(1) For the standard grain size pellets (grain size: 9, 12 μm), the rim structure with sub-divided or recrystallized grains was recognized in the pellet outside to middle region at cross-sectional average burnups above 60 GWd/t. By contrast, it was remarkably suppressed for the two large-grained pellets (37–63 μm) even at high burnups. Almost the same microstructure change was observed for the two standard pellets with almost the same burnup of about 60–61 GWd/t, which had been irradiated in the two types of fuel rods with different diameters and ^{235}U enrichments. This suggests that pellet size and fission rate hardly influence the rim structure formation.

(2) Both fractional recrystallized area observed by TEM and average Xe depression in the pellet outside region measured by EPMA were lower for the large-grained pellets than for the standard pellets, and the two types of large-grained pellets showed remarkable resistance to the rim structure formation. The effect of grain size on the extent of rim structure formation, which was evaluated from the average Xe depression, was expressed as $\propto d^{-0.5}$–$d^{-1.0}$ (d: grain size). This relationship is consistent with the model that grain boundaries act as trapping sites for inhomogeneous dislocation accumulation and then recrystallization localizes near the boundaries. Actually, the present TEM and SEM examinations proved this model.

(3) Although the swelling rate of the two large-grained pellets up to the middle burnup of about 30 GWd/t was larger than that for the standard pellet, it became smaller at higher burnups beyond that burnup.

The lower swelling rate for the large-grained pellets at high burnups was attributed to their milder microstructure change.

(4) Enlarging grain size was effective for suppression of fission gas release. The fission gas releases for the large-grained rods were reduced to about 50–70% of the values for the standard rods, even after base irradiation to rod average burnup of 75 GWd/t. This effect is mainly due to the lower thermally activated release because of a longer diffusion distance of fission gases and partly to higher resistance to the rim structure formation in the large-grained pellets.

Acknowledgements

This study was carried out through the cooperation of Nippon Nuclear Fuel Development Co. Ltd., Japanese Joint Utility Group (Tokyo, Tohoku, Chubu, Hokuriku, and Chugoku Electric Power Corporations and Japan Atomic Power Corp.), Toshiba Corp., Hitachi Ltd. and CRIEPI.

References

[1] S. Sasaki, S. Kuwabara, Proceedings of the International Topical Mtg. on LWR Fuel Performance, Portland, OR, 1997, p. 11.
[2] M.E. Cunningham, M.D. Freshley, D.D. Lanning, J. Nucl. Mater. 188 (1992) 19.
[3] S.R. Pati, A.M. Garde, L.J. Klink, Proceedings of the ANS Topical Mtg. on LWR Fuel Performance, Williamsburg, VA, 1988, p. 204.
[4] R. Manzel, M. Coquerelle, M.R. Billaux, Proceedings of the International Topical Mtg. on LWR Fuel Performance, West Palm Beach, FL, 1994, p. 335.
[5] C.T. Walker, T. Kameyama, S. Kitajima, M. Kinoshita, J. Nucl. Mater. 188 (1992) 93.
[6] R.P. Piron, B. Bordin, G. Geoffrey, C. Maunier, D. Baron, Proceedings of the International Topical Mtg. on LWR Fuel Performance, West Palm Beach, FL, 1994, p. 321.
[7] K. Une, K. Nogita, S. Kashibe, T. Toyonaga, M. Amaya, Proceedings of the International Topical Mtg. On LWR Fuel Performance, Portland, OR, 1997, p. 478.
[8] M. Mogensen, J.H. Pearce, C.T. Walker, J. Nucl. Mater. 264 (1999) 99.
[9] K. Une, K. Nogita, S. Kashibe, M. Imamura, J. Nucl. Mater. 188 (1992) 65.
[10] K. Nogita, K. Une, Nucl. Instrum. and Meth. B 91 (1994) 301.
[11] K. Nogita, K. Une, J. Nucl. Mater. 226 (1995) 302.
[12] K. Une, S. Kashibe, K. Ito, J. Nucl. Sci. Technol. 30 (1993) 221.
[13] M. Hirai, T. Hosokawa, R. Yuda, K. Une, S. Kashibe, K. Nogita, Y. Shirai, H. Harada, T. Kogai, T. Kubo, J.H. Davies, Proceedings of the International Topical Mtg. on LWR Fuel Performance, Portland, OR, 1997, p. 490.
[14] S. Kashibe, K. Une, M. Hirai, Y. Shirai, T. Kogai, T. Kubo, TopFuel'97, Manchester, UK, 1997, p. 5.185.
[15] R. Yuda, H. Harada, M. Hirai, T. Hosokawa, K. Une, S. Kashibe, S. Shimizu, T. Kubo, J. Nucl. Mater. 248 (1997) 262.
[16] J. Spino, K. Vennix, M. Coquerelle, J. Nucl. Mater. 231 (1996) 179.
[17] K. Nogita, K. Une, M. Hirai, K. Ito, K. Ito, Y. Shirai, J. Nucl. Mater. 248 (1997) 196.
[18] M. Mogensen, C. Bagger, C.T. Walker, J. Nucl. Mater. 199 (1993) 85.
[19] C. Ronchi, C.T. Walker, J. Phys. D 13 (1980) 2175.
[20] K. Lassmann, C.T. Walker, J. van de Larr, F. Lindstrom, J. Nucl. Mater. 226 (1995) 1.
[21] K. Lassmann, C.T. Walker, J. van de Larr, J. Nucl. Mater. 255 (1998) 222.
[22] J.O. Barner, M.E. Cunningham, M.D. Freshley, D.D. Lanning, DOE/NE/34046-1, 1990.
[23] K. Mori, K. Watarumi, A. Oe, T. Kurosu, K. Kawasaki, S. Inoue, T. Okubo, Proceedings of the International Topical Mtg. on LWR Fuel Performance, West Palm Beach, FL, 1994, p. 203.
[24] H. Ohara, T. Nomata, M. Irube, M. Futakuchi, S. Iwata, Proceedings of the International Topical Mtg. on LWR Fuel Performance, West Palm Beach, FL, 1994, p. 674.
[25] T.Fujibayasi, S. Koizumi, K. Tsukui, T. Futami, T. Okubo, Y. Mishima, M. Oishi, T. Aoki, IAEA Specialists' Mtg. on Postirradiation Examination and Experience, Tokyo, 1981.
[26] A.H. Booth, CRDC-721, 1958.